International Journal of Pharmaceutics 383 (2010) 244–254

Contents lists available at ScienceDirect

International Journal of Pharmaceutics

journal homepage: www.elsevier.com/locate/ijpharm

Pharmaceutical Nanotechnology

The initial release of cisplatin from poly(lactide-co-glycolide) microspheres

Yan Sim Lee[a], John P. Lowe[b], Ed Gilby[c], Semali Perera[a], Sean P. Rigby[a,*]

[a] Department of Chemical Engineering, University of Bath, Bath BA2 7AY, United Kingdom
[b] Department of Chemistry, University of Bath, Bath BA2 7AY, United Kingdom
[c] Department of Oncology & Radiotherapy, Royal United Hospital, Combe Park, Bath BA1 3NG, United Kingdom

ARTICLE INFO

Article history:
Received 22 June 2009
Received in revised form 8 September 2009
Accepted 14 September 2009
Available online 17 September 2009

Keywords:
PLGA microspheres
In vitro cisplatin release
PFG-NMR
NMR cryoporometry

ABSTRACT

PLGA microspheres loaded with cisplatin were produced using a single emulsion method. A semi-empirical model, with bi-exponential terms, was found to give a better fit to the drug release profiles compared to a mono-exponential model. This model suggests that there are two separate fractions of drug present in the depot. A fraction of the drug is located near/at the surface of the depot, and is readily released during immersion in buffer. A second fraction of drug is entrapped deeper within the depot and is subsequently released. It was also found that the initial release of cisplatin from PLGA microsphere is highly diffusion-controlled and the classical Higuchi model provides a good fit. From studies of water diffusion using PFG-NMR, results suggested that 50:50 PLGA microsphere was most susceptible to swelling and this might have promoted the faster initial drug release. Results from NMR cryoporometry also indicated that the developed PLGA microspheres could have "ink-bottle" pores.

1. Introduction

The key challenge with drug administration is that the plasma drug level should remain at the desired therapeutic level; above which may represent a toxic level, below which the therapeutic effect no longer occurs (Illum, 1987). Ideally, a controlled release system should allow a drug concentration to be maintained at the desired therapeutic level for a prolonged period of time from a single dosage form. Our work aim under the program of New and Emerging Application of Technology (NEAT) project (FSC020), was to develop a controlled drug delivery system that is competent to deliver a standard chemotherapy cisplatin dose. Cisplatin (CPt) is a common cytotoxic drug with proven activity used in chemo-treatment of ovarian cancer (Howell, 2008).

In parallel with the objectives of the NEAT project, the outcomes of the present study should offer an improved understanding of the characteristics of the developed cisplatin-controlled drug delivery system. There is no single, overall mathematical model that covers all the mass transport mechanisms and chemical processes that occur in these disparate systems (Kanjickal and Lopina, 2004). Langer and Peppas (1983) have fundamentally characterised the rate-controlling mechanisms in drug release as diffusion-, swelling- and erosion-controlled processes. Faisant et al. (2002) conveniently categorised the mathematical modelling approaches for degradable devices into two groups: (1) empirical models that assume a first or zero order process controlling the overall drug release; and (2) models considering specific physicochemical phenomena, such as diffusion, mass transfer, or chemical reaction, such as degradation and autocatalytic effects.

First and zero order kinetics, as expressed in Koester et al. (2004), have primarily been adopted to characterise the CPt release profiles of poly(lactide-co-glycolide) (PLGA) samples. In addition, a simplified Higuchi model has also been adopted. The three models are:

$$\text{Zero order kinetic}: Q_t = Q_i + k_z t \quad (1)$$

$$\text{First order kinetic}: \ln Q_t = \ln Q_i + k_F t \quad (2)$$

$$\text{Higuchi model}: Q_t = k_H t^{0.5} \quad (3)$$

where Q_t is the amount of drug released in time, t, and Q_i is the amount of drug within the device at time $t = 0$, k_H is the Higuchi dissolution constant, and k_F and k_z are the first and zero orders rate constants, respectively. The simplified Higuchi model characterises drug release using the effective diffusion coefficient of the soluble component.

In this study, focus was given to the initial phase of drug release, while a semi-empirical model was developed to characterise the overall *in vitro* drug release profile. In order to help understand the characteristics of the developed PLGA microspheres, novel nuclear magnetic resonance (NMR) techniques were used to probe structural evolution of the microspheres.

* Corresponding author. Tel.: +44 1225 38 4978; fax: +44 1225 38 5713.
E-mail address: cesspr@bath.ac.uk (S.P. Rigby).

0378-5173/$ – see front matter © 2009 Elsevier B.V. All rights reserved.
doi:10.1016/j.ijpharm.2009.09.021

1.1. Theory

Quantitative analyses, such as mean pore size, pore size distribution and volume, can be obtained from techniques such as mercury porosimetry and gas adsorption. Mercury porosimetry requires an absolutely dry sample and this technique forces mercury into the pores by applying pressure (Strange, 1994). Mercury will not replace any liquid already in the pores, unless additional pressure is applied to displace the liquid (Ek et al., 1995). Concern is sometimes raised that high pressure might possibly deform a pore (Landry, 2005). Difficulties are also encountered in discriminating between interior pores, and voids between constituent particles, such as with small porous cellulose beads (Ek et al., 1994).

Gas adsorption subjects the sample to *in situ* heating (i.e. ≥100 °C) or degassing for long periods (i.e. ≥12 h) in order to produce an absolutely dry sample. Subsequent analyses utilise weight or volume measurements and, ad- and desorption isotherms to generate pore information. Heating to ≥100 °C is beyond the glass transition temperature (T_g) of PLGA, and it was found difficult to obtain moisture-free PLGA microspheres and accurate weight measurements. Predrying may affect the pore structure due to potential redeposition of dissolved compounds present in the fluid within the porous structure (Collins et al., 2007), and, also, potentially the degradation products in this case. For swell-able solids, pore structures may be different in dry and wet states.

A non-invasive method, such as the aforementioned NMR technique, will therefore be ideal to analyse "wet" samples. In particular, NMR enables the determination of diffusion coefficients for mobile species that can be related to pore information. Pulsed field gradient (PFG)-NMR is a method used to study the self-diffusion of liquids by facilitating the measurement of the root mean square (r.m.s.) displacement of the self-diffusing molecules (Callaghan, 1991). Since the 1960s, PFG-NMR experiments have been used to measure molecular self-diffusion using the attenuated spin echo under the influence of a magnetic field gradient (Stejskal and Tanner, 1965). The details of PFG-NMR can be found elsewhere (Hollewand and Gladden, 1995; Perkins, 2009). Briefly, a series of ^{1}H spectra are collected using a stimulated echo-based pulse sequence that incorporates magnetic field gradients. The strength of the gradients is incremented in each experiment, and the resulting signal intensity is attenuated as the gradient strength is increased.

Free water molecules are always in Brownian motion (Hansen et al., 2005). While self-diffusing water in the bulk demonstrates free diffusion, the diffusion of imbibed liquids is restricted by the walls of the pores. The relationship between the molecular mean square displacement, $\overline{r^2}$, and the molecular self-diffusion coefficient, D_0, is given by the Einstein equation:

$$\overline{r^2} = 6D_0\Delta \tag{4}$$

with Δ as the diffusion time (Veith et al., 2004). For water imbibed within pores or cavities, its diffusion is restricted by the size of the pores/cavities (Callaghan, 1991). For all diffusion to be restricted, Δ must be sufficiently large compared to the pore size. This is because a long diffusion time allows all of the water molecules to reach to the boundary formed by the pore surface. Hence, they are all under restricted diffusion and from the Einstein equation (Eq. (4)): $\Delta \gg (\overline{r^2}/6D)$. Conversely, if Δ is too short, i.e. $\Delta \ll (\overline{r^2}/6D)$, the diffusion time is insufficient for the molecules to diffuse across the pore, and then the measured diffusion coefficient represents the free diffusion because the molecules will not reach to the boundary pore wall (Ek et al., 1994). In an interconnected pore network, after a sufficiently long diffusion time, the diffusivity becomes a measure of the tortuosity of the network.

Following a defined time, the diffusion coefficient, D, of the NMR species can be obtained by 'observing' the positions of the molecules before and after their random diffusion, each being labelled by the magnetic field gradient. The echo attenuation, R, is defined as the ratio of the signal or echo intensity in the presence of the gradient, I, to the echo intensity obtained in the absence of the gradient, I_0 (Hollewand and Gladden, 1995). For free Brownian self-diffusion, where the random motion of the molecules is assumed to be isotropic, R has the function of

$$R = \frac{I}{I_0} = e^{-\gamma^2\delta^2 g^2(\Delta-(\delta/3)-(\tau/2))D} = e^{-D\theta} \tag{5}$$

where γ is the gyromagnetic ratio of the observed nucleus, g is the applied PFG strength, δ is the time of the applied PFG, Δ is the diffusion time, τ is the correction time for the phasing and dephasing between bipolar gradients, and D is the diffusion coefficient. For convenience, the term $\gamma^2\delta^2 g^2[\Delta-(\delta/3)-(\tau/2)]$ will be abbreviated as θ.

For the microsphere experiments herein, it was anticipated that there would be two water components: free water in bulk, and water imbibed within the microspheres (Messaritaki et al., 2005). Hence, considering the two separate diffusion components present, the model now becomes:

$$\frac{I}{I_0} = [pe^{-\theta D_1} + (1-p)e^{-\theta D_2}] \tag{6}$$

where D_1 is the diffusion coefficient of free water in bulk and D_2 is the diffusion coefficient of water imbibed within pores. p is the volume fraction of free water, while $(1-p)$ is the volume fraction of imbibed water.

In addition, NMR cryoporometry has been used to explore the pore geometry of PLGA microspheres, through the study of the melting point depression of a confined liquid (Mitchell et al., 2008). Similar to PFG-NMR, NMR cryoporometry measures the signal from the ^{1}H nuclei within the liquid molecule. The physical property of a confined liquid will deviate from its bulk state because the confinement has introduced new liquid molecules-solid wall interactions. While surface-to-volume ratio (S_v) is affected by the size of a pore, the spin–spin relaxation time of the NMR signal is long for a liquid and short for a solid (Hansen et al., 1996). This enables differentiation between molten and frozen liquids as a function of temperature during freezing.

NMR cryoporometry was developed from the theories of J.W. Gibbs, J. Thomson, W. Thomson and J.J. Thomson, who realised that a different mechanism was involved in a phase transition experienced by a confined material compared to bulk. In particular, they established that the melting point varies inversely with crystal size. A pore of size x will melt at a temperature $T_m(x)$, lower than the bulk melting point T_m, which is inversely proportional to x. As expressed in Mitchell et al. (2008), the Gibbs–Thomson equation relates the melting point depression, ΔT_m, to a small crystal of size x according to

$$\Delta T_m = T_m - T_m(x) = \frac{4\sigma_{sl}T_m}{x\Delta H_f\rho_s} \tag{7}$$

where T_m is the normal bulk melting point, $T_m(x)$ is the melting point of pore of size x, σ_{sl} is the surface energy of the solid–liquid interface, ΔH_f is the enthalpy of fusion, ρ_s is the molar density of the solid. The numerical constant "4" in Eq. (7) is derived for cylindrical pores.

Eq. (7) is a basic model that assumes the pore structure has the same geometry throughout the sample. Assuming all parameters in the equation to be independent of temperature and pore dimension (Hansen et al., 1996), Eq. (7) can be simplified to

$$\Delta T_m = \frac{k}{x} \tag{8}$$

where k is the melting point depression constant associated with the imbibed fluid's thermodynamic properties (Strange, 1994).

Micro- and mesoporous materials can have voids of different geometry; i.e. slit-shaped, cylindrical or spherical, etc. In real samples, the influence of pore geometry is often not uniform. The calibration of this constant is beyond the scope of this study and an appropriate value for PLGA–water system was adopted from Petrov et al. (2006). It is often found that the freezing and melting point depressions are not the same and hysteresis is observed.

Two common freezing mechanisms in porous media are: freezing initiated by nucleation in pores, or by solid-front penetration through pores which are in contact with the frozen bulk (Beurroies et al., 2004). The former is associated with homogeneous nucleation while the latter occurs via heterogeneous nucleation. Here, the freezing in pores is thought to be heterogeneously nucleated by the presence of bulk ice surrounding the microspheres, and the ingress of ice into the microspheres (Hansen et al., 2005; Petrov et al., 2006). This is thought to be the case because a supercooling effect was observed for the bulk water surrounding the PLGA samples.

The aim of the present study was to better understand the *in vitro* cisplatin release from PLGA microspheres. Primarily, NMR techniques were used to study the structural evolution of the biodegradable microspheres, and this information will be related to the "burst release" phase commonly observed in these systems. Hence, this paper is structured as follows: the findings from the *in vitro* drug release are presented; second, the modelling of drug release is presented, and followed by structural studies of the drug-loaded PLGA microspheres. In particular, in this work it will be shown that the generally neglected cryoporometry freezing curve can be used to determine the critical pore neck sizes guarding access to the interior of the microsphere, and that these pore network parameters correlate with mass transport properties. Further, cryoporometry scanning loops will be used to characterise the pore network geometry. It will be shown that these novel NMR techniques allow a greater understanding of the structural evolution underlying the pulse release process to be obtained.

2. Materials and methods

2.1. Materials

50:50, 65:35 and 75:25 PLGA, where the numbers represent the molar ratio of lactide:glycolide, were purchased from Lakeshore Biomaterials Inc., US. Cisplatin (CPt) was purchased from Lianyungang Unionrun Co. Ltd., China. Trifluoromethyl umbelliferone, used for entrapment studies, and platinum standard solution, used for the determination of drug concentration, were purchased from Sigma–Aldrich, UK. Dichloromethane (DCM), used as a solvent, polyvinyl alcohol (PVA), used as an emulsifier in the production of microspheres, and nitric (HNO_3) and hydrochloric (HCl) acids, used as *aqua regia*, were all purchased from Fisher Scientific, UK. An IKA-Ultra-Turrax® T25 homogeniser (Janke & Kunkel GMBH & Co. KG., Germany) was used to produce the emulsion in the microsphere production.

2.2. Production of PLGA microspheres

CPt-loaded 50:50, 65:35 and 75:25 PLGA microspheres were produced using a single emulsion method. Briefly, 10 g of polymer/drug solution were homogenised in 100 ml of PVA solution (0.5%, w/w) at 6500 rpm for 15 min. A polymer concentration of 15% (w/w) and a drug-to-polymer ratio of 1:2 were used. After that, the nascent microspheres were transferred to magnetic stirring at 750 rpm at ambient condition for 3 h. The products were then filtered, washed and air dried. The resulting CPt-loaded microspheres were also sieved into three different size fractions: between 90–75 μm, 75–53 μm and 53–38 μm. Blank 50:50, 65:35 and 75:25 PLGA microspheres were produced using the same method and condition but without drug. For convenience, CPt-loaded 50:50 PLGA microspheres will be abbreviated as CPt-50:50MS henceforth, and similarly for the microspheres made of 65:35 and 75:25 PLGA.

2.3. In vitro drug release analysis

Five preweighed samples were prepared from each PLGA microsphere batch for *in vitro* drug release analysis. Each 0.2 g of microspheres sample was treated in 10 ml of 0.1 M phosphate buffered saline (PBS, pH 7.4). Sample incubation was carried out by shaking in a water bath with a back-and-forth shaking (150 rpm) and temperature maintained at $37.0 \pm 0.5\,^{\circ}C$. Buffer refreshment was carried out hourly for the first 6 h and daily thereafter. At frequent intervals, sample solution was aspirated for CPt content determination (Section 2.4). Results shown are mean ± standard deviation ($n = 5$).

2.4. Determination of CPt concentration

Cisplatin released in the buffer was measured based on the platinum content in the drug molecule using a Model 3110 atomic absorption spectrometer (PerkinElmer Ltd., UK), equipped with a platinum cathode lamp and set at a wavelength (λ) of 265.9 nm to detect platinum concentration. The platinum content in the sample was measured directly by aspirating the sample solution into the spectrometer at a rate of 1.0 ± 0.1 ml/min for 30 s. The cisplatin content was determined from a calibration curve constructed using known platinum concentrations and their corresponding absorbances.

2.5. Determination of drug loading

Acid digestion was used to process CPt-loaded samples. 0.20 g of sample was digested with 4 ml of aqua regia (1:3, HNO_3:HCl) and dried at 85 °C for approximately 45 min to just dryness. This procedure was repeated once or twice in order to achieve complete sample digestion to yield an absolute platinum content. Then 10 ml of 2 M HCl were added to the digested sample and CPt concentration was determined according to Section 2.4. Eq. (9) was used to estimate the drug loading in PLGA microspheres:

$$\text{Drug Loading, DL } (\%) = \left[\frac{\text{Amount of drug (mg)}}{\text{Amount of sample used (mg)}}\right] \times 100\% \quad (9)$$

2.6. Morphological characterisation of PLGA microspheres

A small amount of microspheres were evenly sprinkled onto a carbon adhesive disc mounted onto an aluminium stub. Samples were then coated with a thin layer of gold for 5 min in an Edwards Sputter-coater S150B. The specimen was viewed using a JEOL JSM 6310 scanning electron microscope operating at a typical 10 kV accelerating voltage, 20 °C and 10^{-5} Torr.

2.7. Pulse field gradient (PFG)-NMR experiments

Blank PLGA microspheres were produced according to the method given in Section 2.2. Approximately 0.3 g of sample were immersed in 2 ml of distilled water and then transferred into a 5 mm *ID* NMR tube. ^{1}H NMR with bipolar longitudinal eddy current delay (BPLED) experiments were conducted using a Bruker Advance 400 MHz spectrometer at a probe temperature of 298 K. The measurement of the diffusion coefficient of water was conducted using

a *d*iffusion *o*rdered *s*pectroscop*y* (DOSY) program. DOSY follows the intensity of the stimulated echo signal based on the movement or displacement of a species from one point to another.

For each diffusion measurement, eight ^{1}H spectra (16 scans/datum) were collected at different PFG strengths ranging from 67.40 to 3203.0 Gauss per metre (G/m). The values of Δ, δ and τ used were 0.05 s, 0.002 s, and 0.0001 s, respectively. Each measurement yielded a set of eight intensities (I_{real}), each corresponding to the eight different PFG strengths. I_{calc} was generated by fitting these I_{real} to Eq. (4) using the least-squares method. As aforementioned, in order to obtain a restricted diffusion, the diffusion time, Δ has to be sufficiently large. With a Δ value of 0.05 s, from Eq. (4), the r.m.s. displacement was ~15 μm. This magnitude is likely to exceed the pore sizes but be no larger than the microspheres used in this study, i.e. between 38 and 90 μm.

2.8. NMR cryoporometry

Blank PLGA microspheres were produced according to the method given in Section 2.2. Approximately 1 g of microspheres, comprising the "stock" sample was immersed in 5 ml of distilled water and incubated at 37 °C in a shaking water bath. At specific time interval, a small amount of microspheres was collected using a pipette tip. The top part of the tip was trimmed in order to fit into a NMR tube. The trimmed tip was then inserted into a NMR tube and positioned between a set of susceptibility plugs. A thermocouple used to assess temperature was inserted through the top susceptibility plug to the depth of just reaching the sample. Fresh sample was prepared from the "stock" for each measurement.

Cryoporometry analysis was conducted using the same NMR spectrometer described in Section 2.7, with a spin echo sequence and echo time of 2 ms. The temperature was varied step-wise (0.5 or 1 K/step) within the range of 225–273 K, with a 10 min equilibration time in between changes. The small step change was necessary to ensure temperature stability. The sample was subjected to consecutive cycles of freezing (F-cycle), melting (M-cycle) and refreezing (rF-cycle), or abbreviated as F/M/rF cycles. In doing so, the temperature was reduced step-wise from room temperature to 225 K, then raised to 273 K and reduced again to 225 K. A ^{1}H spin echo spectrum was acquired at each temperature.

A temperature gradient was anticipated to be present along and across the sample. This temperature gradient was minimised by using a set of susceptibility plugs. The plugs raised the sample to within the receiver coil and at the same time, reduced the sample length. Not only did these plugs help to provide insulation for the sample, they also permitted liquid expansion contained in the tip. The NMR experimental conditions used herein were developed by Perkins et al. (2008) and they suggested an error in temperature measurement of 0.2 K was to be expected.

The variation of NMR signal intensity (I) during the F/M/rF cycles was measured as a function of temperature (T) and was plotted as the *IT*-curve. The reasons for using water as the probe fluid are that the water molecules are small enough to enter the minute cavities within the sample and no part of the sample is soluble in water. Allen et al. (2008) found that repeated freezing–thawing often changes the structure of porous materials, while the growth of ice crystals can cause deterioration to the sample. For these reasons, each analysis was done on a fresh sample, though recent results (Perkins et al., 2009) suggest that cryoporometry curves are repeatable for the same sample of microsphere at a given immersion time.

2.9. Confocal laser scanning microscopy (CLSM)

In order to examine the distribution of drug within the microsphere, CLSM was used. PLGA microspheres were produced according to Section 2.2, but with trifluoromethyl umbelliferone (4-TFMU) premixed into the polymer solution. A PLGA-to-4-TFMU ratio of 1:1 was used. A small amount of sample was placed between two glass slides with minimal mineral oil added to hold the cover slides in place. The sample containing-slides were then mounted onto the microscope sample stage. The distribution of entrapped 4-TFMU in PLGA microspheres were observed using a Carl Zeiss LSM 510 (Germany) microscope equipped with an argon photon laser (laser power, 10–75%) with excitation wavelength, λ = 488 nm. The pinhole size was varied from 169 to 1000 μm. Image viewing and processing were performed using LSM 510 software.

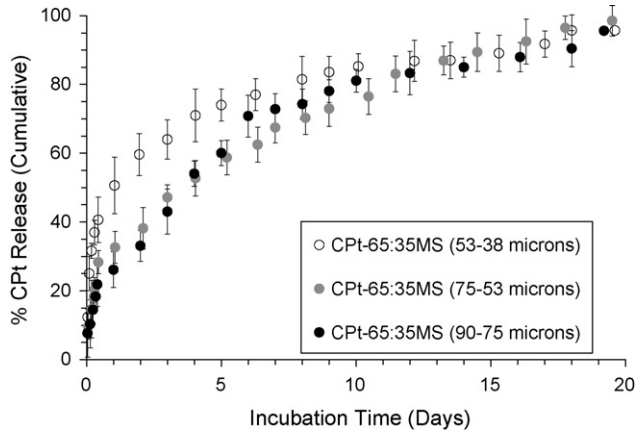

Fig. 1. Percentage (%) cumulative release of CPt from CPt-65:35MS of sizes: 53–38 μm (○), 75–53 μm (●) and 90–75 μm (●).

3. Results

3.1. Studies of in vitro drug release

The drug release in PBS was measured over a period of 20 days for the three PLGA microspheres. As described in Section 2.2, the resultant drug-loaded microspheres were sieved into three different size fractions, namely, 90–75 μm, 75–53 μm and 53–38 μm, in order to study the effect of variation in particle size on drug release. An example of the cumulative *in vitro* drug release profile of CPt-65:35MS is shown in Fig. 1. The drug release profiles of CPt-50:50MS and CPt-75:25MS (result not shown) exhibited similar profiles to those shown in Fig. 1. The drug release profiles of the CPt-loaded PLGA microspheres are fundamentally described as biphasic; Phase 1 is the initial faster drug release during, or up to, the first day, then there is a slower drug release thereafter, denoted as Phase 2.

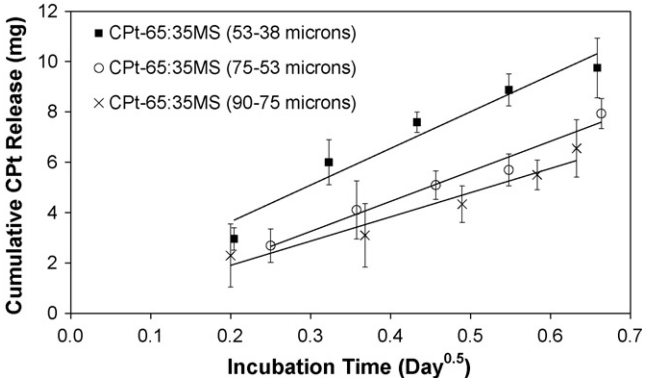

Fig. 2. Cumulative CPt release during the first half a day against square root of time.

3.2. Pharmacokinetics studies

Preliminary attempts to fit Eqs. (1)–(3) to the drug release profiles showed poor modelling of these data. One of the reasons may due to the complication of bulk degrading PLGA where the degradation does not progress at a constant velocity across the sample (Lao et al., 2008). The inadequacy associated with simple empirical models is such that they do not account for any physical conditions, especially the degradation effect on the PLGA drug releasing depots. However, by partitioning the drug release profiles into Phase 1 and Phase 2, it was found that the drug release data during the first 12 h in Phase 1 was, within experimental error, consistent with a Higuchi-type release; an example of CPt-65:35MS is shown in Fig. 2. These results suggest that the initial release of CPt from the PLGA microspheres produced in this work during the first 12 h, is diffusion-controlled.

To attempt to improve the modelling of CPt release profiles, a semi-mechanistic model was used. This model can be used to relate the parameters of the rate equation to the physical conditions of the depots. As described by Machida et al. (2000), the drug released in solution is related to the ultimate amount of drug released from the depot by

$$Q_1 = Q_0(\infty)(1 - e^{-k_0 t}) \quad (10)$$

where Q_1, the amount of drug released into solution at time, t, which is dependent upon the release constant, k_0, and $Q_0(\infty)$ is the amount of drug ultimately released from the depot.

A second exponential term can be added to the model based on an approach using a three compartmental model. The model now contains a releasing depot with two pools. Physically, the first pool may represent a fraction of drug that is located near/at the surface of the depot and is readily released. The second pool represents subsequent drug release arising from those molecules entrapped deeper within the matrix. The model (Machida et al., 2000) describing the relationship between the amount of drug released and the ultimate amounts of drug released from the two pools of the depot is

$$Q_1 = [Q_2(\infty)(1 - e^{-k_2 t})] + [Q_3(\infty)(1 - e^{-k_3 t})] \quad (11)$$

where Q_1 is the amount of drug released into the solution. $Q_2(\infty)$ and $Q_3(\infty)$ are the ultimate amounts of drug released from Pools A and B, which will be released after a long time. k_2 and k_3 are the release rate constants of Pools A and B, respectively. Both Eqs. (10) and (11) were fitted to the experimental data and examples of the results are shown in Fig. 3. From Fig. 3 it can be seen that the data for CPt-75:25MS give a much better fit to a single exponential model than the data for the other two types of microspheres. However, data for all three types of microspheres show a better fit to a bi-exponential model.

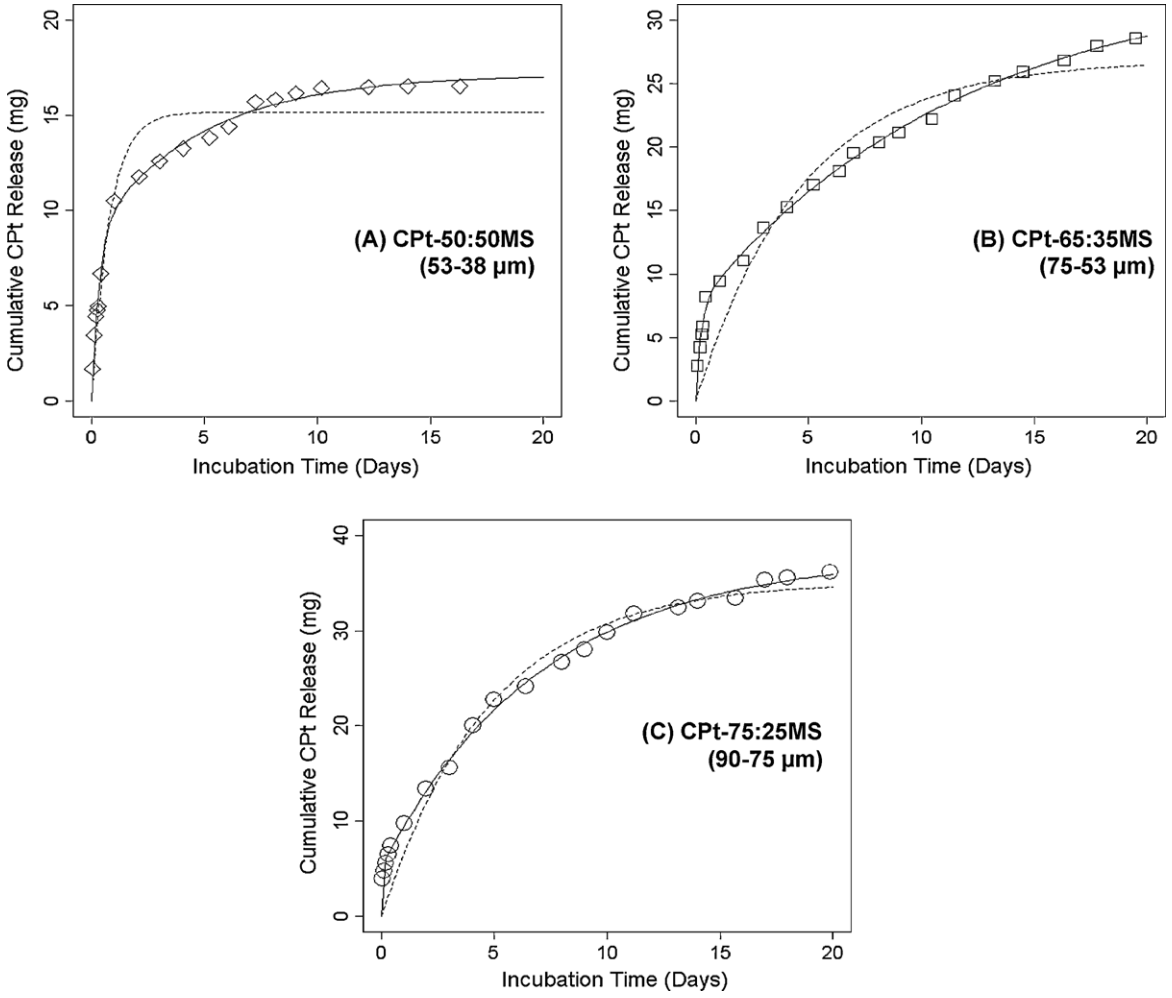

Fig. 3. Examples of model Eq. (10) and (11) fittings to CPt release profiles of: (A) CPt-50:50MS (53–38 μm), (B) CPt-65:35MS (75–53 μm), (C) CPt-75:25MS (90–75 μm). Solid lines represent the bi-exponential model (Eq. (11)), while dashed lines represent the mono-exponential model (Eq. (10)). Error bars were omitted for clarity.

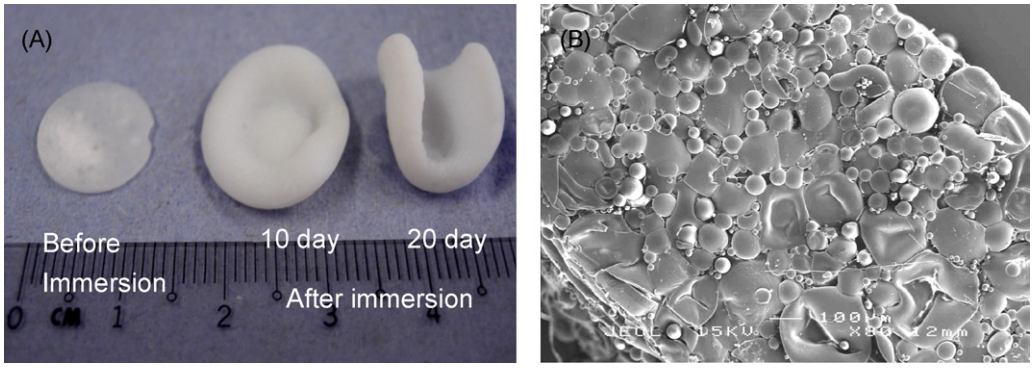

Fig. 4. (A) 65:35MS-disc before and, after 10 days and 20 days immersion in water. (B) SEM image of 65:35MS-disc.

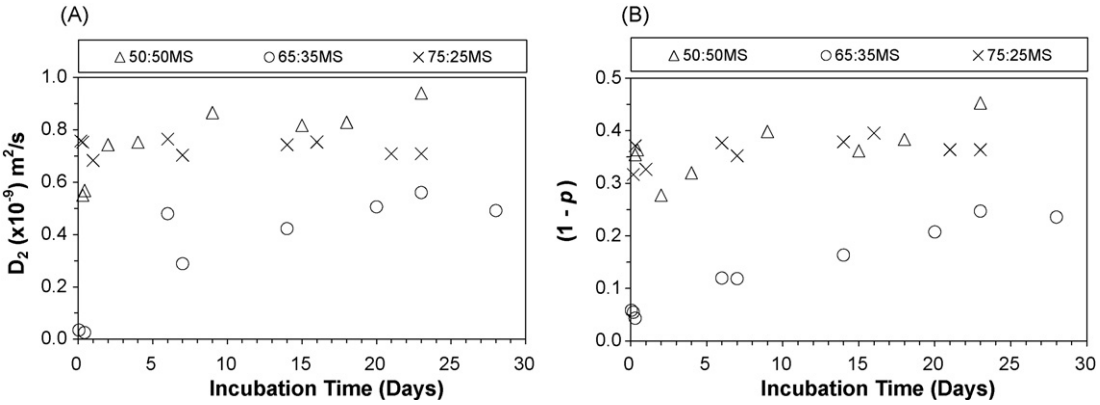

Fig. 5. (A) The diffusion coefficient of imbibed water, D_2 and (B) the volume fraction of imbibed water $(1-p)$ of 50:50MS (△), 65:35MS (◯) and 75:25MS (×).

3.3. Studies of water transport in PLGA microspheres

Swelling of the device is common for PLGA microspheres (Matsumoto et al., 2006). Fig. 4 shows 65:35MS-discs produced using high pressure pressing. Fig. 4 proves that 65:35MS underwent hydration and the disc had swollen after 10 and 20 days immersion in water. Fig. 4B shows the fragility of PLGA microsphere towards high pressure disc-pressing. The partially deformed 65:35MS could lead to a hydration gradient across the disc.

The estimated diffusion coefficients of imbibed water (D_2) in PLGA microspheres and their corresponding volume fraction of imbibed water $(1-p)$ are shown in Fig. 5. It should be noted that there is approximately 0.4% of uncertainty associated with the measurement of diffusion coefficient using PFG-NMR due to inhomogeneity in the magnetic field (Kato et al., 2006). Perkins (2009) suggested that the error in the model could be as high as 5%. The relatively constant values of D_2 and $(1-p)$ for 75:25MS suggest that significantly less structural evolution is occurring in these microspheres when compared with the 50:50MS and 65:35MS. This may explain why the drug-release data for the 75:25MS gives a much better fit to a mono-exponential (single (drug release) phase) model when compared with the data for the 50:50MS and 65:35MS.

Fig. 6 shows the F-cycles of 75:25MS after immersion in water for various times. Referring to the significant decrease in signal intensities shown in Fig. 6, the bulk liquid was frozen at 266–267 K (denoted as T_{Fo}). The F-cycle following 5 days immersion of 75:25MS exhibits a diminutive step just above 260 K and another at ~240 K. The F-cycle, following 10 days of immersion for 75:25MS, exhibits a clear step close to T_{Fo} and another at ~241 K. The F-cycle from 20 days 75:25MS exhibits a gradual decrease in I/I_{273} below T_{Fo} and a step at ~240 K. I_{273} is the signal intensity measured at 273 K. The 30 days 75:25MS exhibits the most distinct pattern where a clear and prominent step close to T_{Fo} can be seen followed by another at ~240 K.

In some cases, the values of I/I_{273} are observed to be higher than unity. This is attributable to the varying I_{273}. Since I was detected based on the presence of molten water in molten phase and is indicative of its volume in bulk, over time, the bulk water diffuses into the microspheres and thus reduces the prior measured I_{273}. It should also be noted that the measured NMR intensity is temperature dependent due to Boltzman's effect. The Boltzmann statistics shows that the ratio of NMR proton spins, with upper- and lower-energy states are temperature dependent (Mitchell et al., 2008).

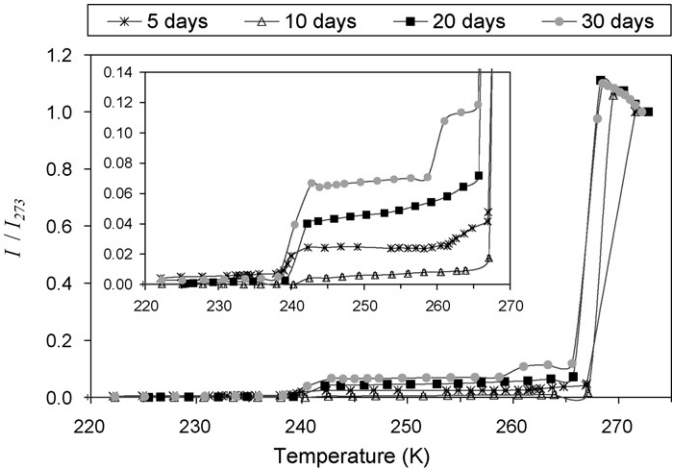

Fig. 6. *IT* curves for the F-cycles of 75:25MS after immersion in water for 5, 10, 20 and 30 days. Inset: A refocus on the lower scale of I/I_{273}.

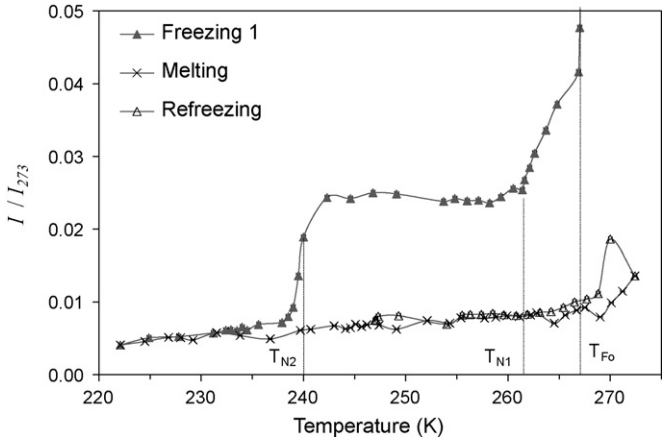

Fig. 7. *IT* curves for F/M/F cycles of 75:25MS after 5 days immersion in water.

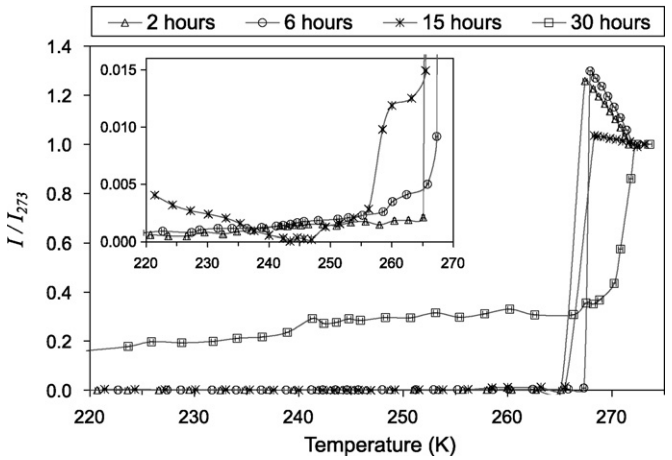

Fig. 8. *IT* curves for freezing cycles of 50:50MS after 2, 6, 15 and 30 h immersion in water. Inset: A refocus on the lower scale of I/I_{273}.

The measured intensity, I (T_K), at absolute temperature, T_K can be corrected relative to the signal intensity, I (273 K), at 273 K based on the Curie Law using:

$$\frac{I(T_K)}{I(273\ K)} = \frac{273}{T_K} \tag{12}$$

The measured intensities of cryoporometry experiments were corrected using Eq. (12) and the results show that the temperature effect was minimal on the measured intensities.

Fig. 7 shows the F/M/rF cycles obtained from 75:25MS after 5 days immersion in water. The plot focused on the lower scale of I/I_{273} in order to show the small variations in I/I_{273} with temperature. After Freezing 1 (F-cycle), the frozen sample was subjected to a subsequent melting (M-cycle) but the temperature was raised only to a point just below the bulk melting point (i.e. ≤273 K) while the bulk remained frozen. Following that, a rF-cycle was initiated. Following the F-cycle, the bulk liquid was first frozen at ~267 K. Second and third freezing transitions occurred at ~258.5 K (T_{N1}) and ~239 K (T_{N2}), respectively. For convenience, the notations such as 'N1' and 'N2' are used to describe the relative temperatures to T_{Fo}; i.e. T_{N1} is closer to T_{Fo} while T_{N2} is further away from T_{Fo}. With both the F/M cycles, it shows that the confined water in 75:25MS underwent supercooling. The larger nano-pores, freezing at ~260 K, must have direct access to the surface bulk liquid, while the smaller pores froze at ~240 K. The significant reduction in hysteresis between the melting curve and the refreezing scanning loop suggest that narrow necks with relatively little pore volume guard access to the interior of the microspheres.

The F-cycles obtained from 50:50MS after immersion in water for various times are shown in Fig. 8. The sampling time point of 50:50MS was based on a hourly basis in view of the more rigid sample before any degradation effect commences, which might complicate interpretation of the results. The F-cycle from 50:50MS after 2 h immersion in water did not exhibit any clear step below T_{Fo} (~266 K). Based on the enlarged plot (shown in inset), the F-cycle of 6 h water-immersed 50:50MS exhibits a step at ~258 K. The F-cycle from 50:50MS after 15 h immersion in water exhibits a clear step at ~255 K. Thereafter, fluctuation in signal occurred at a magnitude close to the background signal and no further interpretation could be derived. For the 30 h-immersed 50:50MS, its F-cycle tends to show a step at ~266 K and another at ~240 K.

The F-cycles shown in Fig. 8 demonstrate the difficulty of interpreting precise information purely based on the *IT*-curve. Since the liquid volume is related to the measured intensity, the *IT* curves represent the pore volume as a function of temperature (Strange, 1994). The information of interest, in this case, the pore size distribution can be quantitatively determined by studying the distribution of these freezing temperatures. The pore volume, $V(x)$ is a function of pore diameter x and the volume of pores with diameter between $(x + \Delta x)$ is $(dv/dx)\Delta x$. The pore size distribution can then be determined using the measurement dV/dx provided k is known for the liquid use.

A range of k values for water, as probe liquid, measured using different silica beads are available in the literature such as, i.e. 52 K nm (Hansen et al., 1996; Morishige and Kawano, 1999), and 50 K nm from a work involving PLGA microspheres (Petrov et al., 2006). The particular problems with polymeric microspheres are the influences of swelling and degradation, both of which will alter the physical structure and properties of the measured sample. Ideally, the influence of these variations ought to be accounted for in the k calibration. For this work, a k value of 50 K nm will be used to estimate the neck sizes and their corresponding freezing temperatures based on the F-cycles using Eq. (8). The results are presented in Tables 1 and 2. 273.15 K was used as the normal freezing temperature for water and not the measured freezing point obtained from specific sample which was suppressed by the supercooling effect.

3.4. Distribution of entrapped agent in PLGA microsphere

The results from this experiment can mimic the distribution of entrapped drug in PLGA microspheres and can be related to the drug release pattern of PLGA microspheres (Rigby et al., 2004; Messaritaki et al., 2005). Fig. 9A shows multiple 75:25MS, while individual 75:25MS are shown in Fig. 9(B) and (C). Fig. 9(B) and

Table 1
The estimated freezing points and necks sizes of 75:25MS after immersion in water.

Immersion in water (day)	First freezing transition		Second freezing transition	
	Temperature, T_{N1} (K)	Neck size, x_{N1} (nm)	Temperature, T_{N2} (K)	Neck size, x_{N2} (nm)
5	261.4	4.31	239.5	1.49
10	–	–	240.3	1.52
20	–	–	239.2	1.47
30	265.6	6.76	238.2	1.43

Table 2
The estimated freezing points and necks sizes of 50:50MS after immersion in water.

Immersion in water (h)	Estimated temperature (K)	Estimated neck size (nm)
	T_{N1}	x_{N1}
2	265.1	6.33
6	267.3	8.77
15	265.5	6.67
30	238.9	1.47

(C) clearly indicate a heterogeneous distribution pattern of the entrapped 4-TFMU based on the spatial variation in fluorescence intensities.

By "stacking" sequential two-dimensional (2D) micrographs, collected for planes located at different depths through the specimen, the spatial distribution of entrapped 4-TFMU in 75:25MS can be studied. The three-dimensional (3D) projections of a 75:25MS entrapped with 4-TFMU are shown in Fig. 10; with orthogonal views of the sphere and sequential 2D micrographs focused at different depth planes. The depth of the image plane is indicated on the top left corner of the micrograph; i.e. 0 μm indicates the image plane was at the periphery of the sphere; 1 μm indicates the image plane was 1 μm into the sphere from its periphery.

Fig. 10 shows a 75:25MS of size ~20 μm. From Fig. 10C, it can be seen that the spatial distribution of 4-TFMU varied across the sphere. For instance, with the increasing intensity from plane distance of 0 to 4–5 μm, this indicates an increase in concentration of the entrapped agent across these planes. From the orthogonal view (Fig. 10B), the distinct bright site tends to concentrate at one side of the sphere. Regions filled with 4-TFMU could vary in intensity over time due to probable water transport between the interior cavities.

4. Discussion

Fig. 1 shows the cumulative *in vitro* release of CPt from CPt-65:35MS of different size fractions. CPt-65:35MS of the smallest size fraction (53–38 μm) clearly exhibits the fastest drug release rate compared to other size fractions. For example, CPt-65:35MS of the smallest size fraction released up to 40% of its drug content during the first day whereas CPt-65:35MS with larger fractions did not reach to 40% drug release after 2 days. After approximately 12 days, the drug released from CPt-65:35MS of all size fractions tended to converge and proceed at a similar rate. The smallest size fraction CPt-65:35MS is likely to have the largest S_v ratio and therefore, it was anticipated that they should exhibit a faster drug release rate. In contrast, microspheres of larger size would exhibit a lower rate

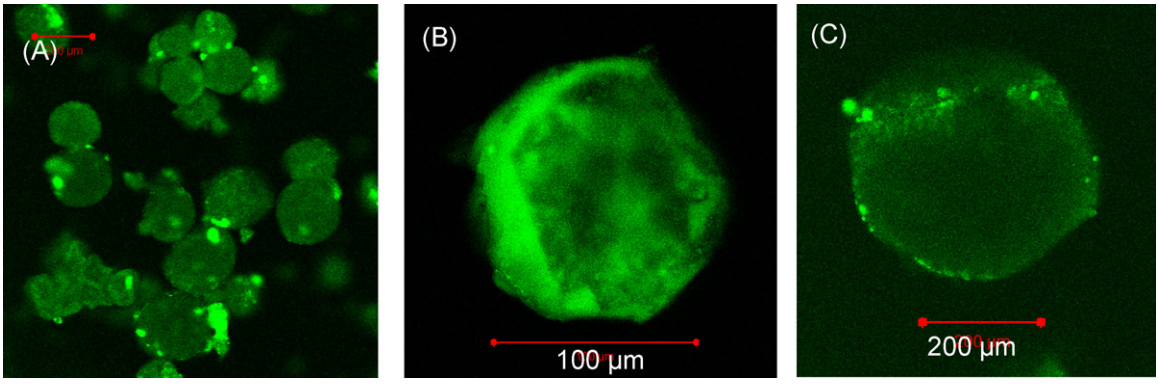

Fig. 9. Confocal micrographs focused at equatorial plane showing (A) multiple 75:25MS, and (B) to (C) singular 75:25MS entrapped with 4-TFMU.

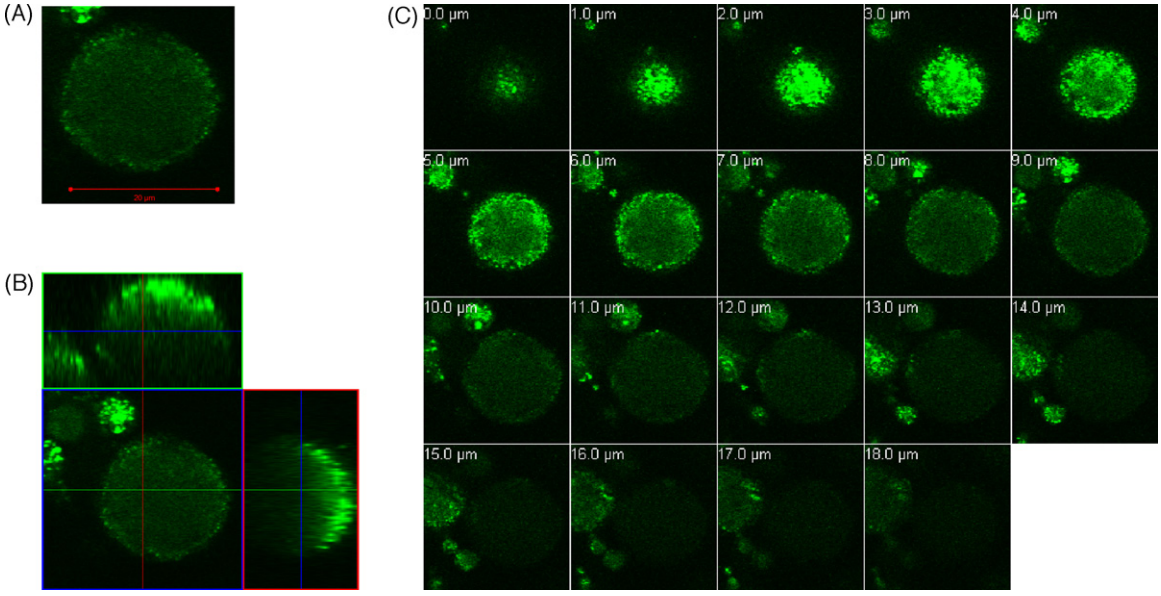

Fig. 10. Confocal micrographs showing the cross-sections of a 75:25MS entrapped with 4-TFMU; (A) at equatorial plane, (B) orthogonal views and (C) cross-sections at different plane depth.

of drug release due to the longer diffusion path length across the larger sphere.

The initial drug release during Phase 1 is associated with a rapid release phase commonly known as the "burst release". Burst release can be defined as the quantity of drug that escapes from microparticles prior to the onset of polymer erosion-mediated drug release (Allison, 2008a). An instant cumulative CPt release as high as 25% in PLGA microspheres has been reported (Fujiyama et al., 2003). The fittings of the Higuchi model ($Q_t = k_H t^{0.5}$), shown in Fig. 2, suggested that the Phase 1 drug release is highly diffusional.

During microsphere production, the drug can show a tendency to diffuse towards the aqueous phase (Perez et al., 2000). This leads to entrapment of CPt in the periphery of the microspheres, and causes an increased drug concentration at the periphery. This further creates a large drug concentration gradient between the microspheres and buffer during buffer immersion. The large concentration gradient subsequently provides a greater driving force for drug diffusion. In addition, during the production process, free CPt from leakage might have adsorbed on the surface of the microspheres. These CPt molecules are then easily released into the buffer. Other factors that can contribute to rapid drug release are such as the pore dimensions within the microparticles, the polymer matrix density and the particle porosity. Meanwhile, the termination of burst release may be explained by structural relaxation due to increased particle density and surface pore closure (Allison, 2008b).

In some cases, the microspheres of intermediate and largest size fractions exhibited similar release rates. Possible effects may arise from: (1) the different local concentration of the drug within a microsphere which can influence the drug release pattern (Matsumoto et al., 2005). Drug located in the outermost periphery of the microspheres would be expected to be rapidly released. CLSM studies (Section 3.4) show a heterogeneous spatial distribution of the entrapped agent in PLGA microsphere. Similar results were obtained by Messaritaki et al. (2005). (2) While hindering a homogeneous drug distribution, the different amorphous regions in PLGA can also affect the freedom of drug diffusion within the matrix, in addition to contributing to a rapid drug release (Sastre et al., 2004).

The CPt release from CPt-65:35MS could be related to the gradual increase in D_2 and $(1-p)$ for 65:35MS (Fig. 5A). This hydration profile obtained from PFG-NMR experiments mimics the CPt release from 65:35MS seen in Fig. 1. The gradual hydration within 65:35MS provides medium for drug transport such that drug can be released into the buffer. The greater changes in the D_2 and $(1-p)$ parameters over time for the 65:35MS compared to the 75:25MS suggest that greater structural evolution is occurring in the 65:35 MS, which may be associated with the larger observed changes in the drug release rate.

The fast Phase 1 drug release observed in CPt-50:50MS during the first day may be correlated to the microsphere swelling profile seen in Fig. 5A. During swelling of a microsphere, its glass transition temperature is lowered (Hopfenberg and Hsu, 1978), and buffer immersion (Siepmann et al., 2004) shifts the physical state of the system to a rubbery state which permits faster medium diffusion (Fan and Singh, 1989). Siepmann et al. (2004) also found that this shift was independent of microsphere size.

CPt release from PLGA microspheres cannot be fully characterised by empirical models (Eqs. (1)–(3)) and it has been reported in the literature that PLGA microparticles can yield a non-square root relation drug release profile (Fujiyama et al., 2003). A complex model developed by Grassi et al. (2000) accounted for the factors such as the sizes of the particles, the physical state and distribution of the entrapped drug within the device, including the dissolution and diffusion of the drug. Jalil and Nixon (1990) proposed a number of relevant mechanisms such as surface-drug desorption, drug diffusion through particle pores and various regions in the polymer matrix. It is common for a model to have specific components that are mechanism- and time-dependent during the release period (Liu et al., 2006; Duarte et al., 2006). However, the contribution of these mechanisms can sometimes be difficult to quantify (Polakovič et al., 1999).

Both Eqs. (10) and (11) were fitted to the CPt release profiles and examples of results are shown in Fig. 3. Goodness of fit was compared based on the Akaike's Information Criterion (AIC) factor. In all cases, the AIC values of the model described by Eq. (11) were lower compared to those of Eq. (10). The distribution of residual plots also shows a random distribution about the zero-axis. Hence, the bi-exponential Eq. (11) is suggested to be more suitable to fit to the CPt release profiles compared to a mono-exponential model. This also implies that the developed PLGA devices can be described as a depot having two pools; the first pool contains a readily released fraction of drug, and the remaining will be subsequently released at a later stage.

During the initial measurements, D_2 for both 50:50MS and 75:25MS (Fig. 5A), are well above those of 65:35MS, suggesting 65:35MS experienced lower rate of hydration. This is reflected in the lower fraction of imbibed water $(1-p)$ for 65:35MS seen in Fig. 5B. The D_2 of 50:50MS began with a lower value than that of 75:25MS but after 4 days, it surpassed the D_2 of 75:25MS. A possible scenario is that, initially, the pores within 50:50MS were the most tortuous, and then water started to diffuse into the microspheres. As a result, pore expansion and swelling increased the fraction of imbibed water. The effects of hydration on PLGA microspheres are proposed below:

i. Hydration occurs via two phases, water diffusion through the amorphous region of the polymeric microsphere and water penetration through surface micro- or nano-pores. This hydration process will increase the fraction of imbibed water $(1-p)$. Prior to this, the microspheres may be partially filled with residual water from the production process.
ii. When a cavity or pore undergoes hydration, it expands and leads to swelling. As a result, the microsphere can increase in size (Fig. 4A).
iii. The presence of interconnecting channels or amorphous regions would permit water transport between pores or regions in the matrix.

In the event of water diffusing from one pore to another, i.e. from bigger pores to smaller pores, while the water in a bigger pore leaves to fill a smaller pore, the "swollen" bigger pore decreases in size while the smaller pore expands as water gradually fills up. These lead to temporary changes in pore sizes where pores expand and shrink due to water migration between them. Furthermore, it could also be that initially, the pores nearest to the microsphere surface experience a more frequent hydration-swelling effect. This effect then gradually took place in the interior of the spheres as immersion proceeded.

Here, it is suggested that the least hydrophobic nature and degradation resistance of 50:50MS gives rise to a higher water diffusion compared to 65:35MS and 75:25MS. Hence, D_2 increases with $(1-p)$ because of the higher hydration rate experienced by 50:50MS. Thus, the imbibed water was able to move more freely in enlarging pores.

It is common to observe that swell-able polymeric microspheres exhibit both structural swelling and shrinking. Fujiyama et al. (2003) presented cross-sectional SEM images of degrading PLGA/PLA microspheres. Interior structural collapse was shown by these authors and at different degradation times, this structure alternated between dense and porous natures. Swelling was thought to have caused the expansion of local cavities/pores and

minimised the adjacent spaces. The pore sizes of swollen cellulose beads after immersion in water could sometimes double their initial sizes (Ek et al., 1995).

Owing to its higher S_v ratio, liquid confined within pores crystallises (or freezes), and melts, at temperatures well below its bulk melting point. Compared to bulk, this high S_v ratio introduces excess energy for the solid. Thereby, the liquid–solid equilibrium is shifted towards the liquid state (Petrov and Furó, 2006). Hence, molten liquid is still present in the porous microspheres even below the normal freezing point of water. The freezing of water in pores occurs via the ingress of ice crystals from the frozen bulk into the interior pores (Khokhlov et al., 2007; Perkins et al., 2008) and this causes the delay in the complete freezing of water present in the system, as seen in Figs. 6–8. This scenario resembles the typical "ink-bottle" pores where the main pores are connected through "necks" of smaller sizes.

In order to overcome the nucleation barrier that may delay freezing, Brun et al. (1977) suggested to initially freeze the system with excess liquid and at a low enough temperature to obtain a frozen bulk. Following that, the temperature is increased to a point just below the bulk melting temperature to study melting in pores. Subsequently, freezing is initiated again. By doing so, a solid phase will always exists at the entrance of the pores and can act as nuclei for freezing inside pores.

The resulting F/M/rF cycles (Fig. 7) show that the signal intensities of the latter two cycles were very close to the background signal/noise and were unable to clearly distinguish any phase changes for a large fraction of the pore size distribution. This scenario may be because the 75:25MS used had pore sizes such that their corresponding melting points were very close to the bulk melting temperature.

It is also evident that the F/M cycles shown in Fig. 7 did not retrace one another thereby suggesting the presence of hysteresis. This is largely due to the delayed freezing nucleation (Petrov and Furó, 2006). By referring to Fig. 7, the mechanism, whereby the freezing of water confined in pores occurs by ice ingress from the frozen bulk through the interconnecting channels, can be demonstrated. For porous media, the hysteresis is thought to have originated from the pores of varying cross-sections and networks effects. It is the connection through a smaller channel to a bigger main cavity that gives rise to pore-blocking effect. This mechanism occurs when a narrow channel is preventing the further ingress of the solid phase. After reaching T_{Fo}, the ice front will not be able to ingress into smaller pores until the thermodynamical condition favouring this penetration is achieved. Consequently, a second or third freezing point is detected at a much lower temperature.

The following theories are suggested by Petrov and Furó (2006) to explain the freezing/melting hysteresis;

i. As far as bulk liquid is concerned, homogenous nucleation causes an uncontrollable delay in freezing. The bulk liquid becomes supercooled until homogeneous nucleation initiates freezing.
ii. Freezing by solid ingress within the interior pores may be heterogeneously nucleated by the surrounding bulk ice but this solid ingress is delayed by a pore-blocking effect.
iii. There is present a free-energy barrier for solid ingress which separates metastable states of a confined material from stable ones.

This sort of analysis is advanced from the studies of capillary condensation and vaporisation which are parallel to those of melting and solidification/freezing respectively (Beurroies et al., 2004; Denoyel et al., 2004). From the delay in freezing (Fig. 7), the following is deduced:

i. 75:25MS are likely to be porous and hydration enables water to be imbibed in its interior.
ii. The presence of hysteresis suggested that these pores are made of ink-bottle geometry. The ink-bottle effect is thought to delay the freezing of confined water.
iii. Since melting curves could not be explored, the freezing curves can only be used to estimate the size of the neck, i.e. the "channels" through which the ice crystal ingresses. The presence of second and third freezing points indicated a bimodal system; 75:25MS used herein was potentially inherited with necks of one or two different sizes.

Referring to Fig. 7, when the temperature reaches T_{N1}; this point corresponds to the freezing of the water in the interconnecting neck of size x_{N1}. Further cooling to T_{N2} freezes the water in the neck of size x_{N2}. From the Gibbs–Thomson equation (Eq. (7)), the neck with size x_{N1} is bigger than the neck with size x_{N2} because the latter occurs at a lower temperature.

The same mechanism observed in liquid freezing can be expected for melting of liquid in porous media inherited with ink-bottle pores (Beurroies et al., 2004). Since the water confined in pores will not freeze before the water in its connecting necks, likewise, the melting will also begin in the neck before the frozen confined water. Denoyel and Pellenq (2002) also agreed with this phenomenon, suggesting that surface melting occurs at the end of the metastable range and the only condition is that the pore wall is preferentially wetted by the liquid rather than by the solid phase (ice). Morishige and Kawano (1999), amongst others, also observed the presence of a bound liquid layer located adjacent to the pore wall when the inner fluid had frozen.

For the necks present in 75:25MS, only the 5 and 30 days samples show a bimodal neck size system. The appearance and disappearance of the smaller necks in 75:25MS could have been caused by the swelling/shrinking effects. Hansen et al. (2005) discovered a complicating situation in which changes could appear in the porous network upon the addition of water. During their sample preparation, the drying process caused the pores to partially shrink, and in extreme cases, collapse. In subsequent measurement, some of the larger pores that collapsed during the earlier drying reappeared after water immersion. In 75:25MS, although pores of size x_{N1} were not detected on the tenth and twentieth days, they may reappear at different stages. The expansion of smaller space within the polymeric matrix could also be forming new necks, while the swollen necks transformed into larger cavities/pores and disappeared from the detection.

For 50:50MS, they are observed to have a unimodal neck-pore system. Again, the intermittent polymer swelling and shrinkage may have given rise to the increase and decrease in their neck sizes. After 30 h of immersion in water, a much smaller neck size, i.e. 1.47 nm, was detected. This neck could be a newly expanded space due to polymeric swelling, or a neck that is experiencing shrinking effect. Our further results (not shown) from NMR cryoporometry experiments showed that 50:50MS can be experiencing more prominent swelling effects and the appearance of second necks at a much later stage.

Fig. 10 shows a 75:25MS of size ~20 μm. From Fig. 10C, it can be seen that the spatial distribution of 4-TFMU varied across the sphere. For instance, with the increasing intensity from plane distance of 0 to 4–5 μm, this indicates an increase in concentration of the entrapped agent across these planes. From the orthogonal view (Fig. 10B), the distinct bright site tends to concentrate at one side of the sphere, which was the bottom hemisphere. This is attributable to the presence of residual water. Regions filled with 4-TFMU could vary in intensity over time due to possible water transport between the interior cavities.

Figs. 9 and 10 show the heterogeneous distribution of 4-TFMU in 75:25MS. The amorphous and crystalline regions in PLGA are thought to hinder a homogeneous distribution of entrapped agent (Sastre et al., 2004). An imperfect entrapment can arise from an unstable emulsion during the production process. This instability can lead to the coalescence of droplets and can cause the drug to be heterogeneously distributed within the microsphere (Perez et al., 2000). As aforementioned, the heterogeneous distribution of entrapped agent in PLGA microsphere can contribute to the complexity in predicting *in vitro* drug release.

With the suggested swell-able and bimodal neck system inherited by the PLGA microspheres produced in this study, drug may be entrapped in the main pores with small connecting necks. These drugs would not be released until the connecting necks undergo swelling to permit the passage of drug. This mechanism of the neck might contribute to the applicability of a bi-exponential model (Eq. (11)), which indicates the presence of two separate drug fractions.

Acknowledgements

This work is funded by the Department of Health, UK under the NEAT program (FSC020), and is in collaboration with the Royal United Hospital (RUH), Bath. The authors wish to thank the Department of Health, UK, and Avon Cancer Unit at RUH for their generous financial support. Also, special thanks extend to the gynaecology team; Mr. Nick Johnson and Miss. Tracy Miles at the RUH for their support.

References

Allen, S.G., Stephenson, P.C.L., Strange, J.H., 2008. Internal surfaces of porous media studied by nuclear magnetic resonance cryoporometry. J. Chem. Phys. 108, 8195–8198.
Allison, S.D., 2008a. Analysis of initial burst in PLGA microparticles. Exp. Opin. Drug Deliv. 5, 615–628.
Allison, S.D., 2008b. Effect of structural relaxation on the preparation and drug release behavior of poly(lactic-co-glycolic) acid microparticle drug delivery systems. J. Pharm. Sci. 97, 2022–2035.
Beurroies, I., Denoyel, R., Llewellyn, P., Rouquerol, J., 2004. A comparison between melting-solidification and capillary condensation hysteresis in mesoporous materials: application to the interpretation of thermoporometry data. Thermochim. Acta 421, 11–18.
Brun, M., Lallemand, A., Quinson, J.-F., Eyraud, C., 1977. A new method for the simultaneous determination of the size and the shape of pores: the thermoporometry. Thermochim. Acta 21, 59–88.
Callaghan, P.T., 1991. Principles of Nuclear Magnetic Resonance Microscopy. Oxford University Press, Oxford.
Collins, J.H.P., Gladden, L.F., Hardy, I.J., Mantle, M.D., 2007. Characterizing the evolution of porosity during controlled drug release. Appl. Magn. Reson. 32, 185–204.
Denoyel, R., Pellenq, R.J.M., 2002. Simple phenomenological models for phase transitions in a confined geometry. 1. Melting and solidification in a cylindrical pore. Langmuir 18, 2710–2716.
Denoyel, R., Beurroiesa, I., Lefevre, B., 2004. Thermodynamics of wetting: information brought by microcalorimetry. J. Petrol. Sci. Eng. 45, 203–212.
Duarte, A.R.C., Costa, M.S., Simplıcio, A.L., Cardoso, M.M., Duarte, C.M.M., 2006. Preparation of controlled release microspheres using supercritical fluid technology for delivery of anti-inflammatory drugs. Int. J. Pharm. 308, 168–174.
Ek, R., Henriksson, U., Nystrom, C., Odberg, L., 1994. Pore characterization in cellulose beads from diffusion studies using the spin echo NMR technique. Powder Technol. 81, 279–286.
Ek, R., Lennholm, H., Davidson, R., Nystrom, C., 1995. Pore swelling in beads made of cellulose fibres and fibre fragments. Int. J. Pharm. 122, 49–56.
Faisant, N., Siepmann, J., Benoit, J.P., 2002. PLGA-based microparticles: elucidation of mechanisms and a new, simple mathematical model quantifying drug release. Eur. J. Pharm. Sci. 15, 355–366.
Fan, L.T., Singh, S.K., 1989. Diffusion-controlled release. In: Fan, L.T., Singh, S.K. (Eds.), Controlled Release: A Quantitative Treatment. Publisher: Springer, Berlin.
Fujiyama, J., Nakasea, Y., Osaki, K., Sakakura, C., Yamagishi, H., Hagiwara, A., 2003. Cisplatin incorporated in microspheres: development and fundamental studies for its clinical application. J. Control. Rel. 89, 397–408.
Grassi, M., Colombo, I., Lapasin, R., 2000. Drug release from an ensemble of swellable crosslinked polymer particles. J. Control. Rel. 68, 97–113.
Hansen, E.W., Fonnum, G., Weng, E., 2005. Pore morphology of porous polymer particles probed by NMR relaxometry and NMR cryoporometry. J. Phys. Chem. B 109, 24295–24303.
Hansen, E.W., Schmidt, R., Stocker, M., 1996. Pore structure characterization of porous silica by ^{1}H NMR using water, benzene and cyclohexane as probe molecules. J. Phys. Chem. 100, 11396–11401.
Hollewand, M.P., Gladden, L.F., 1995. Transport heterogeneity in porous pellets. I. PGSE NMR studies. Chem. Eng. Sci. 50, 309–326.
Hopfenberg, H.B., Hsu, K.C., 1978. Swelling controlled and constant rate delivery systems. Polym. Eng. Sci. 18, 1186–1191.
Howell, S.B., 2008. Pharmacologic principles of intraperitoneal chemotherapy for the treatment of ovarian cancer. Int. J. Gynecol. Cancer 18, 20–25.
Illum, L., 1987. In: Illum, L., Davis, S.S. (Eds.), Polymers in Controlled Drug Delivery. Publisher: Wright, Bristol.
Jalil, R., Nixon, J.R., 1990. Microencapsulation using poly(L-lactic acid): release properties of microcapsules containing phenobarbitone. J. Microencapsul. 7, 53–66.
Kanjickal, D.G., Lopina, S.T., 2004. Modeling of drug release from polymeric delivery systems—a review. Crit. Rev.™ in Therapeutic Drug Carrier Systems 21, 345–386.
Kato, H., Saito, T., Nabeshima, M., Shimada, K., Kinugasa, S., 2006. Assessment of diffusion coefficients of general solvents by PFG-NMR: investigation of the sources error. J. Magn. Reson. 180, 266–273.
Khokhlov, A., Valiullin, R., Kärger, J., Steinbach, F., Feldhoff, A., 2007. Freezing and melting transitions of liquids in mesopores with ink-bottle geometry. New J. Phys. 9, 272–279.
Koester, L.S., Ortega, G.G., Mayorga, P., Bassani, V.L., 2004. Mathematical evaluation of in vitro release profiles of hydroxypropylmethylcellulose matrix tablets containing carbamazepine associated to b-cyclodextrin. Eur. J. Pharm. Biopharm. 58, 177–179.
Landry, M.R., 2005. Thermoporometry by differential scanning calorimetry: experimental considerations and applications. Thermochim. Acta 433, 27–50.
Langer, R., Peppas, N., 1983. Chemical and physical structure of polymers as carriers for controlled release of bioactive agents: a review. J. Macromol. Sci. 23, 61–126.
Lao, L.S., Venkatraman, S.S., Peppas, N.A., 2008. Modeling of drug release from biodegradable polymer blends. Eur. J. Pharm. Biopharm. 70, 796–803.
Liu, C., Desai, K.C.H., Tang, X., Chen, X., 2006. Drug release kinetics of spray-dried chitosan microspheres. Dry. Technol. 24, 769–776.
Machida, Y., Onishi, H., Kurita, A., Hata, H., Morikawa, A., Machida, Y., 2000. Pharmacokinetics of prolonged-release CPT-11-loaded microspheres in rats. J. Control. Rel. 66, 159–175.
Matsumoto, A., Matsukawa, Y., Suzuki, T., Yoshino, H., 2005. Drug release characteristics of multi-reservoir type microspheres with poly(DL-lactide-co-glycolide) and poly(DL-lactide). J. Control. Rel. 106, 172–180.
Matsumoto, A., Matsukawa, Y., Horikiri, Y., Suzuki, T., 2006. Rupture and drug release characteristics of multi-reservoir type microspheres with poly(DL-lactide-co-glycolide) and poly(DL-lactide). Int. J. Pharm. 327, 110–116.
Messaritaki, A., Black, S.J., van der Walle, C.F., Rigby, S.P., 2005. NMR and confocal microscopy studies of the mechanisms of burst drug release from PLGA microspheres. J. Control. Rel. 108, 271–281.
Mitchell, J., Webber, J.B.W., Strange, J.H., 2008. Nuclear magnetic resonance cryoporometry. Phys. Reports 461, 1–36.
Morishige, K., Kawano, K., 1999. Freezing and melting of water in a single cylindrical pore: the pore-size dependence of freezing and melting behavior. J. Chem. Phys. 110, 4867–4872.
Perez, M.P., Zinutti, M., Lamprecht, A.L., Ubrich, N., Astier, A., Hoffman, M., Bodmeier, R., Maincent, P., 2000. The preparation and evaluation of poly(e-caprolactone) microparticles containing both a lipophilic and a hydrophilic drug. J. Control. Rel. 65, 429–438.
Perkins, E.L., 2009. Nuclear Magnetic Resonance Studies of Drug Release Devices. PhD Thesis, University of Bath, United Kingdom.
Perkins, E.L., Lowe, J.P., Edler, K.J., Tanko, N., Rigby, S.P., 2008. Determination of the percolation properties and pore connectivity for mesoporous solids using NMR cryodiffusometry. Chem. Eng. Sci. 63, 1929–1940.
Perkins, E.L., Lowe, J.P., Edler, K.J., Rigby, S.P., 2009. Studies of structure-transport relationships in biodegradable polymer microspheres for drug delivery using NMR cryodiffusometry. Chem. Eng. Sci., doi:10.1016/j.ces.2009.06.036.
Petrov, O., Furó, I., 2006. Curvature-dependent metastability of the solid phase and the freezing-melting hysteresis in pores. Physical Review E 73, 011608.
Petrov, O., Furó, I., Schuleit, M., Domanig, R., Plunkett, M., Daicic, J., 2006. Pore size distributions of biodegradable polymer microparticles in aqueous environments measured by NMR. Int. J. Pharm. 309, 157–162.
Polakovič, M., Gorner, T., Gref, R., Dellacherie, E., 1999. Lidocaine loaded biodegradable nanospheres. II. Modelling of drug release. J. Control. Rel. 60, 169–177.
Rigby, S.P., van der Walle, C.F., Raistrick, J.H., 2004. Determining drug spatial distribution controlled delivery tablets using MFX imaging. J. Control. Rel. 96, 97–110.
Sastre, R.L., Blanco, M.D., Teijón, C., Olmo, R., Teijón, J.M., 2004. Preparation and characterisation of 5-flurouracil-loaded Poly(ε-Caprolactone) Microspheres for Drug Administration. Drug Develop. Res. 63, 41–53.
Siepmann, J., Faisant, N., Akiki, J., Richard, J., Benoit, J.P., 2004. Effect of the size of biodegradable microparticles on drug release: experiment and theory. J. Control. Rel. 96, 123–134.
Stejskal, E.O., Tanner, J.E., 1965. Spin diffusion measurements: spin echoes in the presence of a time dependent field gradient. J. Chem. Phys. 42, 288–292.
Strange, J.H., 1994. Cryoporometry: a new NMR method for characterising porous media. Nondestr. Test. Eval. 11, 261–271.
Veith, S.R., Hughes, E., Vuataz, G., Pratsinis, S.E., 2004. Restricted diffusion in silica particles measured by pulsed field gradient NMR. J. Colloid Interface Sci. 274, 216–228.